

Graphene Spin Transistor

Sungjae Cho, Yung-Fu Chen[†] and Michael S. Fuhrer*

*Department of Physics and Center for Superconductivity Research, University of
Maryland, College Park, Maryland 20742, USA*

*to whom correspondence should be addressed: mfuhrer@umd.edu

[†]present address: Department of Physics, 1110 West Green, Urbana, IL 61801-3080,
USA

Graphitic nanostructures, e.g. carbon nanotubes (CNT) and graphene, have been proposed as ideal materials for spin conduction¹⁻⁷; they have long electronic mean free paths⁸ and small spin-orbit coupling⁹, hence are expected to have very long spin-scattering times. In addition, spin injection and detection in graphene opens new opportunities to study exotic electronic states such as the quantum Hall^{10,11} and quantum spin Hall⁹ states, and spin-polarized edge states¹² in graphene ribbons. Here we perform the first non-local four-probe experiments¹³ on graphene contacted by ferromagnetic Permalloy electrodes. We observe sharp switching and often sign-reversal of the non-local resistance at the coercive field of the electrodes, indicating definitively the presence of a spin current between injector and detector. The non-local resistance changes magnitude and sign quasi-periodically with back-gate voltage, and Fabry-Pérot-like oscillations^{6,14,15} are observed, consistent with

quantum-coherent transport. The non-local resistance signal can be observed up to at least $T = 300$ K.

Figure 1 describes the spin-valve device (see Methods). Figure 1b shows the gate voltage (V_g) dependence of the resistivity ρ and conductivity σ . Similar to other single- and bi-layer graphene devices^{10,16} $\sigma(V_g)$ shows a broad minimum around $4e^2/h$, where e is the electronic charge and h Planck's constant, increasing linearly with V_g away from the minimum at V_{cnp} (the charge neutrality point, CNP).

Figure 2a shows the four-probe non-local resistance $R_{\text{nl}} = V_{\text{nl}}/I$ (see Figures 1c,d) as a function of magnetic field B at $V_g = +70$ V. R_{nl} is positive at large B . As B is swept to negative, R_{nl} remains positive as B crosses zero, then switches to a negative value at $B \approx -150$ G before returning positive at $B \approx -250$ G. Upon sweeping B positive, switching occurs at $B = +150$ G and $+250$ G. This behavior is very similar to that observed in all-metal^{13,17-19} and CNT²⁰ non-local spin-valves, particularly the sign change of R_{nl} when the current and voltage circuits are separated^{19,20}. Hence we identify these two magnetic fields as the coercive fields of F4 and F3 respectively. The switching behavior may then be explained as follows: at high B , F3 preferentially injects its majority spin which diffuses to F4 and is detected as an increase in the chemical potential of F4's majority spin (since the magnetizations of F3 and F4 are parallel) resulting in positive R_{nl} . When F3 and F4 are antiparallel, the voltage reverses, and R_{nl} is negative.

Figure 2b,c,d shows the same measurement performed at different gate voltages and different electrode arrangements. In Figures 2b,d, the high- B value is negative, and R_{nl} switches to near zero (or slightly positive) for B between the two coercive fields. The sign change is discussed further below. Figures 2e,f show the memory effect: two R_{nl}

states can be observed at $B = 0$, corresponding to the two possible magnetization states of the low-coercivity electrode.

First we discuss whether R_{nl} arises due to charge current or spin current flowing between F3 and F4. Ideally, charge current would flow only between F3 and F2, eliminating contributions to the R_{nl} from magnetoresistance of the ferromagnetic electrodes (anisotropic magnetoresistance), the channel, or the electrode-channel interface. However, because R_{nl} is ~ 3 orders of magnitude smaller than the device resistance, it is possible that some charge current flows through a tortuous path from F3 to F4 and F5. We investigate this by measuring the gate voltage and temperature dependence of R_{nl} .

Figure 3a shows the gate voltage dependence of R_{nl} in the parallel and antiparallel state, $R_{nl,p}$ and $R_{nl,ap}$, as well as their average value. Figure 3b shows the non-local spin-valve signal ΔR . R_{avg} , $R_{nl,p}$ and $R_{nl,ap}$ all show a peak near the CNP ($10 \text{ V} < V_g < 30 \text{ V}$), while ΔR is near zero in this region. Well outside this region ($V_g < -20$ or $V_g > 40 \text{ V}$), $R_{nl,p}$ and $R_{nl,ap}$ have nearly equal magnitude and opposite sign (R_{avg} is near zero) and ΔR is larger and shows quasi-periodic oscillations with V_g . The peak in $R_{avg}(V_g)$ near the CNP suggests that charge current *does* flow in the region between F3 and F4 for these gate voltages. However, $R_{avg}(V_g)$ is not simply proportional to $\rho(V_g)$ but rather drops to near zero at large V_g while $\rho(V_g)$ remains finite. Thus the finite $R_{avg}(V_g)$ near the CNP is likely due to the inhomogenous nature of graphene near the CNP^{21,22}; here percolating electron and hole regions may cause a tortuous current path.

Away from the CNP, $R_{avg}(V_g)$ drops to near zero, indicating small charge current. Yet $R_{nl,p}$ and $R_{nl,ap}$ remain finite, with near equal magnitude and opposite sign. This is as

expected for a pure spin current flowing from F3 to F4, and cannot be explained by a magnetoresistive signal arising from any charge current between F4 and F5. The Hall effect is another possible source of V_{nl} , however, the Hall voltage would be expected to grow large and switch sign near the CNP, rather than showing a peak.

Figure 4 shows the temperature dependence of R_{avg} and ΔR for $V_g = 0$. Here R_{avg} is finite similar to Figure 3, but somewhat larger for this electrode configuration. The spin-valve signal ΔR is seen to drop with temperature approximately as $\Delta R \propto T^{-1}$, while R_{avg} is much more weakly temperature dependent; again indicating a different origin for ΔR and R_{avg} . The inset shows a measurement at 300 K performed at higher current; the spin-valve signal can still be observed, confirming expectations of reduced spin scattering in graphene even to high temperature.

We now discuss the magnitude of the spin-valve signal ΔR . For an Ohmically-contacted spin-valve device, the non-local signal may be estimated using Eqn. 22 of reference [17]; we estimate in this case the signal should be on order $10^{-5} \Omega$. However, we observe finite contact resistance of order 10 k Ω per electrode as estimated from the difference between two-probe and four-probe resistance measurements. In the limit of highly resistive contacts, we would expect the non-local resistance to be given by Eqn. 2 of reference [19], which, for long spin-scattering lengths, is on the order of the channel resistance (1-10 k Ω). Our intermediate contact resistance, finite spin-scattering length, and finite polarization of the electrodes will give a lower value of ΔR , similar to the observation of $\Delta R \sim 20 \Omega$ for a channel resistance 10 k Ω and contact resistance of a few tens of k Ω in a CNT device²⁰.

We now discuss the origins of the quasi-periodic oscillations of the non-local spin-valve signal $\Delta R(V_g)$. Oscillation of the spin-valve signal with V_g due to spin-orbit coupling has been proposed as the basis of a spin transistor²³. However, the spin-orbit coupling in graphene is expected to be very small⁹, and this effect should not be observable²⁴. Oscillations and sign changes of the spin-valve signal have also been observed when the spin current flows through a resonant quantum state, either due to Coulomb blockade²⁵ or resonant tunneling⁶. It is evident from Figure 1b that the sample is not in the Coulomb blockade regime, however $\rho(V_g)$ shows quasi-periodic oscillations. We examined similar oscillations in another graphene sample in a two-probe geometry, (Figure 4c). In the color-scale plot of differential conductance vs. V_g and drain voltage V , conductance maxima and minima occur along diagonal lines. In CNTs, such behavior is attributed to Fabry-Pérot interference of electronic states reflected from the electrodes^{6,14}, and similar behavior has been reported in graphene¹⁵. The round trip phase experienced by an electron traveling the CNT channel varies by 2π when the change in electron

wavenumber is $\Delta k = \pi/L$. This results in a period in gate voltage $\Delta V_g = \frac{2}{L} \left(\frac{\pi e V_g'}{c_g} \right)^{1/2}$ and

in drain voltage $\Delta V = \frac{h v_F}{e L}$. The slope of the lines is

$$\frac{\Delta V}{\Delta V_g} = \frac{2c_g}{e^2} \frac{1}{D(E)} = h v_F \left(\frac{c_g}{4\pi e^3 V_g'} \right)^{1/2},$$

where $v_F = 1 \times 10^6$ m/s is the Fermi velocity, and

$V_g' = |V_g - V_{\text{cnp}}|$. For this device, $L = 200$ nm, $V_{\text{cnp}} \approx -6$ V, giving $\Delta V = 20$ mV. For $V_g' = 10$ -15 V, we find $\Delta V_g = 2.0$ -2.5 V, and the slope varies from 0.013 to 0.010. The slopes match quite well the experimentally observed slopes (see Figure 3c). The most prominent minima in conductivity at $V = 0$ occur with spacing $\Delta V_g = 1.5$ -2.5 V, however

additional features are observed more closely spaced in V and V_g than expected from above. This is not surprising due to the two-dimensional nature of graphene: our analysis includes only the k -states perpendicular to the electrodes, undercounting the states involved in transport (the slope is independent of the path length L). The spin-valve sample also shows oscillations of $\sigma(V_g)$ in Figure 1b. For this sample $L = 450$ nm, and we would expect $\Delta V_g = 2.8$ V at $V_g' = 90$ V (i.e. $V_g = -70$ V) which agrees reasonably well with the observed spacing of dips $\Delta V_g \sim 6$ V at large negative V_g in Figure 1b. The four-probe geometry is significantly more complicated than the two-probe analysis of Fabry-Pérot interference above, since there are multiple interfaces which could give rise to interference. Still it is reasonable that quantum interference effects are responsible for the oscillations in the four-probe resistivity (Figure 1b), and for the observed changes in magnitude and sign of the spin-valve signal with gate voltage (Figure 3b).

In conclusion, we have observed the non-local resistance arising from a spin current in graphene in a non-local four-probe measurement. The spin-valve signal varies with gate voltage in magnitude and sign due to interference arising from the quantum-coherent transport through graphene, which is also evidenced by Fabry-Pérot-like interference patterns observed in a similar sample, and oscillations in the four-probe resistivity of the spin-valve sample. The magnitude of the spin-valve signal is roughly inversely proportional to temperature, and is observable at room temperature. Injection and detection of pure spin currents in graphene opens possibilities to examine theoretically predicted new phenomena such as the spin Hall effect⁹ and half-metallicity in graphene ribbons¹². Because of the high current-carrying capability and long mean-

free path at room temperature, graphene is also an excellent candidate for room-temperature spintronics applications.

Acknowledgements

This work has been supported by the U.S. ONR grant N000140610882, NSF grant CCF-06-34321, and the UMD-NSF-MRSEC grant DMR-05-20471.

Methods

Our graphene samples are obtained by mechanical exfoliation²⁶ on 300 nm SiO₂/Si substrates. We use optical microscopy to locate the graphene and verify single-layer thickness²⁷; the optical contrast is compared with other samples fabricated on identical substrates which show the half-integer quantum Hall effect characteristic of graphene^{10,11,21}. We estimate that all the samples discussed in this manuscript are at most two graphene layers thick. Ferromagnetic Permalloy electrodes are formed by electron-beam lithography (EBL) followed by thermal evaporation; a second EBL step establishes contact to the Permalloy via normal Cr/Au electrodes.

References

1. Cottet, A. et al. Nanospintronics with carbon nanotubes. *Semiconductor Science and Technology* **21**, S78-S95 (2006), and references therein.
2. Hill, E. W., Geim, A. K., Novoselov, K., Schedin, F. & Blake, P. Graphene Spin Valve Devices. *IEEE Trans. Magn.* **42**, 2694-2696 (2006).
3. Tsukagoshi, K., Alphenaar, B. W. & Ago, H. Coherent transport of electron spin in a ferromagnetically contacted carbon nanotube. *Nature* **401**, 572 (1999).
4. Orgassa, D., Mankey, G. J. & Fujiwara, H. Spin injection into carbon nanotubes and a possible application in spin-resolved scanning tunnelling microscopy. *Nanotechnology* **12**, 281-284 (2001).

5. Thamankar, R. et al. Spin-polarized transport in magnetically assembled carbon nanotube spin valves. *Applied Physics Letters* **89**, 033119-3 (2006).
6. Man, H. T., Wever, I. J. W. & Morpurgo, A. F. Spin-dependent quantum interference in single-wall carbon nanotubes with ferromagnetic contacts. *Physical Review B (Condensed Matter and Materials Physics)* **73**, 241401-4 (2006).
7. Chen, Y.-F. Semiconducting Carbon Nanotube Transistors: Electron and Spin Transport Properties. *Ph.D. Thesis, University of Maryland* (2006).
8. Dürkop, T., Kim, B. M. & Fuhrer, M. S. Properties and applications of high-mobility semiconducting nanotubes. *Journal of Physics: Condensed Matter* **16**, R553-R580 (2004).
9. Kane, C. L. & Mele, E. J. Quantum Spin Hall Effect in Graphene. *Physical Review Letters* **95**, 226801-4 (2005).
10. Novoselov, K. S. et al. Two-dimensional gas of massless Dirac fermions in graphene. *Nature* **438**, 197-200 (2005).
11. Zhang, Y., Tan, Y.-W., Stormer, H. L. & Kim, P. Experimental observation of the quantum Hall effect and Berry's phase in graphene. *Nature* **438**, 201-204 (2005).
12. Son, Y.-W., Cohen, M. L. & Louie, S. G. Half-metallic graphene nanoribbons. *Nature* **444**, 347-349 (2006).
13. Jedema, F. J., Filip, A. T. & van Wees, B. J. Electrical spin injection and accumulation at room temperature in an all-metal mesoscopic spin valve. *Nature* **410**, 345-348 (2001).
14. Liang, W. et al. Fabry-Perot interference in a nanotube electron waveguide. *Nature* **411**, 665-9 (2001).
15. Miao, F., Wijeratne, S., Coskun, U., Zhang, Y. & Lau, C. N. Phase Coherent Transport of Charges in Graphene Quantum Billiard. *Condensed Matter Archive*, 0703052 (2007).
16. Novoselov, K. S. et al. Unconventional quantum Hall effect and Berry's phase of 2π in bilayer graphene. *Nature Physics* **2**, 177 (2006).
17. Jedema, F. J., Nijboer, M. S., Filip, A. T. & van Wees, B. J. Spin injection and spin accumulation in all-metal mesoscopic spin valves. *Physical Review B (Condensed Matter and Materials Physics)* **67**, 085319-16 (2003).
18. Jedema, F. J., Nijboer, M. S., Filip, A. T. & vanWees, B. J. Spin Injection and Spin Accumulation in Permalloy–Copper Mesoscopic Spin Valves. *Journal of Superconductivity: Incorporating Novel Magnetism* **15**, 27 (2002).
19. Garzon, S., Zutic, I. & Webb, R. A. Temperature-Dependent Asymmetry of the Nonlocal Spin-Injection Resistance: Evidence for Spin Nonconserving Interface Scattering. *Physical Review Letters* **94**, 176601-4 (2005).
20. Tombros, N., Molen, S. J. v. d. & Wees, B. J. v. Separating spin and charge transport in single-wall carbon nanotubes. *Physical Review B* **73**, 233403 (2006).
21. Cho, S. & Fuhrer, M. S. Charge Transport and Inhomogeneity near the Charge Neutrality Point in Graphene. *condmat/0705.3239* (2007).
22. Adam, S., Hwang, E. H., Galitski, V. M. & Sarma, S. D. A self-consistent theory for graphene transport. *Condensed Matter Archive*, 0705.1540 (2007).
23. Datta, S. & Das, B. Electronic analog of the electro-optic modulator. *Applied Physics Letters* **56**, 665-667 (1990).

24. De Martino, A. & Egger, R. Rashba spin-orbit coupling and spin precession in carbon nanotubes. *Journal of Physics: Condensed Matter* **17**, 5523-5532 (2005).
25. Sahoo, S. et al. Electric field control of spin transport. *Nature Physics* **1**, 99 (2005).
26. Novoselov, K. S. et al. Two-dimensional atomic crystals. *Proceedings of the National Academy of Sciences* **102**, 10451–10453 (2005).
27. Abergel, D. S. L., Russell, A. & Fal'ko, V. I. Visibility of graphene flakes on a dielectric substrate. *condmat/0705.0091* (2007).

Figure Captions

Figure 1 Graphene spin-valve device. **a**, Optical micrograph of graphene on SiO₂/Si substrate. Scale bar is 10 microns, white box shows the graphene flake used in this study, which has similar contrast to other graphene samples for which half-integer quantum Hall effect was measured. **b**, Gate voltage (V_g) dependence of four-probe resistivity ρ (black, left scale) and conductivity σ (blue, right scale) at a temperature of 1.25 K. The field-effect mobility $\mu_{FE} = (1/c_g)|d\sigma/dV_g|$ is approximately 2500 cm²/Vs, where $c_g = 1.15 \times 10^{-4}$ F/m² is the gate capacitance. In this local resistivity measurement, electrodes F4 and F5 were used as voltage probes, and the current contacts were F3 and F6. **c,d**, Schematics of device layout. **c**, Plan view. **d**, Side view, showing setup for non-local resistance measurement. Six ferromagnetic Permalloy electrodes F1-F6 were deposited on top of the graphene strip. To give different coercive fields, F1, F3, F5 have dimensions 0.4 μm x 15 μm , and F2, F4, F6 are 1.0 μm x 3 μm . Spaces between all the electrodes are 450nm.

Figure 2 Non-local spin-valve effect in graphene. **a,b**, Nonlocal resistance R_{nl} (see **Figure 1d**) as a function of magnetic field measured at temperature $T = 20\text{K}$ with current $I = 100$ nA. **a,b** F2, F3 as current leads; F4, F5 voltage leads. **c,d** F4, F5 as current leads; F2, F3 voltage leads. **a**, Gate voltage $V_g = +70$ V. **b**, $V_g = -67$ V. **c**, Gate voltage $V_g = -20$ V. **d**, $V_g = -69$ V. The non-local resistance switches sign upon sweeping magnetic field, which indicates that a spin current flows from electrodes F3 to F4 (see **Figure 1c,d**). The reversal of sign of the non-local resistance with gate voltage (**a** vs. **b** and **c** vs. **d**) is discussed in the text and in **Figure 3**. **e,f**, Memory effect measured at $T =$

20 K, $I = 100$ nA, $V_g = 0$ V. F1, F2 are current leads; F3, F4 are voltage leads. In **a-f**, blue curves correspond to positive sweep direction of magnetic field; black curves, negative sweep direction.

Figure 3 Gate-voltage dependence of spin-valve signal. **a**, Resistance as a function of gate voltage for electrodes with magnetizations parallel ($R_{nl,p}$), antiparallel ($R_{nl,ap}$), and their average $R_{avg} = (R_{nl,p} + R_{nl,ap})/2$. **b**, The spin valve signal $\Delta R = R_{nl,p} - R_{nl,ap}$ as a function of gate voltage. **a,b**, The same electrode configuration is used as for **Figure 2a,b**. **c**, Color-scale plot of two-probe differential conductance as a function of gate voltage V_g and drain voltage V for a similar graphene sample contacted by Permalloy electrodes with a spacing 200 nm. The blue and red dashed lines have slopes of ± 0.013 and ± 0.010 respectively.

Figure 4. Temperature dependence of spin-valve signal. The average resistance R_{avg} (black circles) and spin valve signal ΔR (blue squares) as a function of temperature at $V_g = 0$ V and $I = 100$ nA. The temperature dependence of the spin-valve signal ΔR is much stronger than that of R_{avg} (which likely arises from the charge-current resistance). The solid line shows a power law with exponent -1. Inset shows the non-local resistance R_{nl} as a function of field at $T = 300$ K and $I = 3$ μ A. Blue curve is positive sweep direction of magnetic field; black curve, negative sweep direction. The spin-valve effect is still observable. The electrodes used for the spin-valve data in main panel and inset are the same as for **Figure 2e,f**.

Figure 1

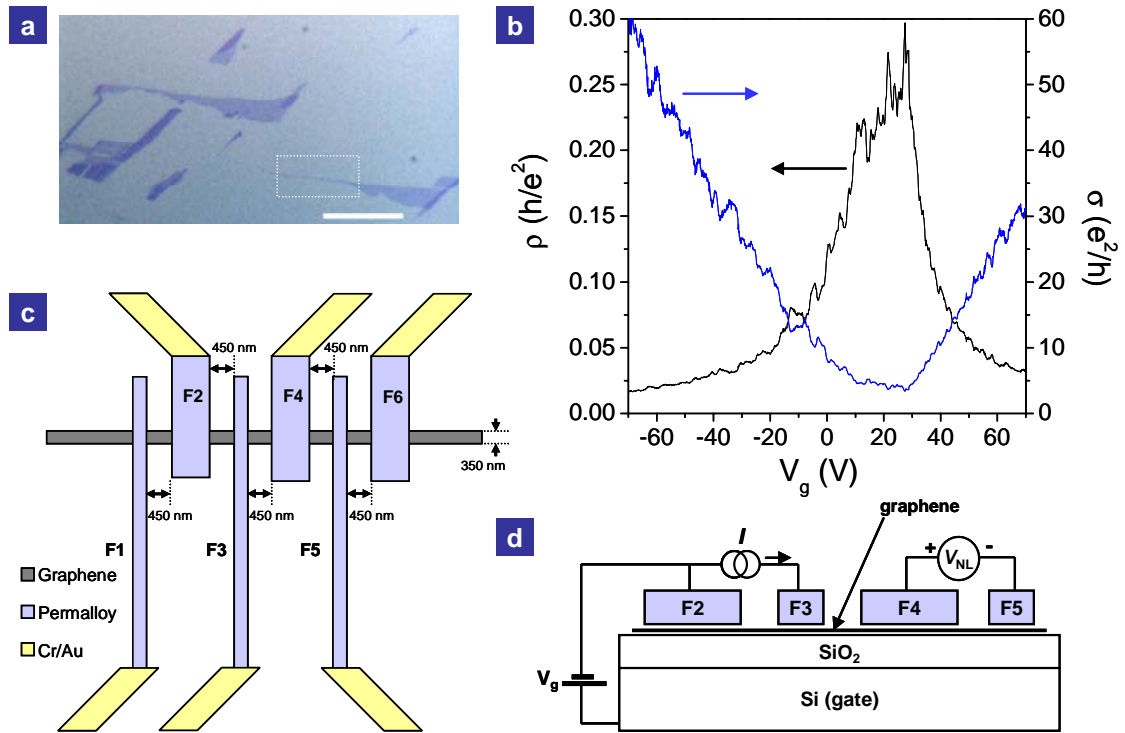


Figure 2

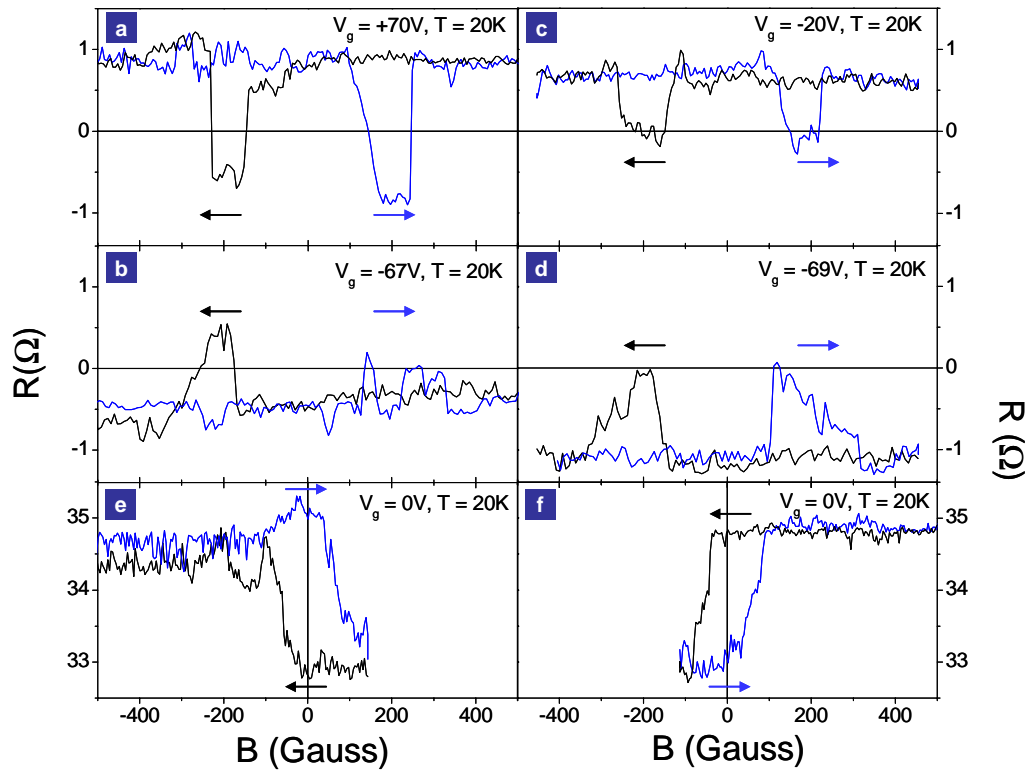


Figure 3

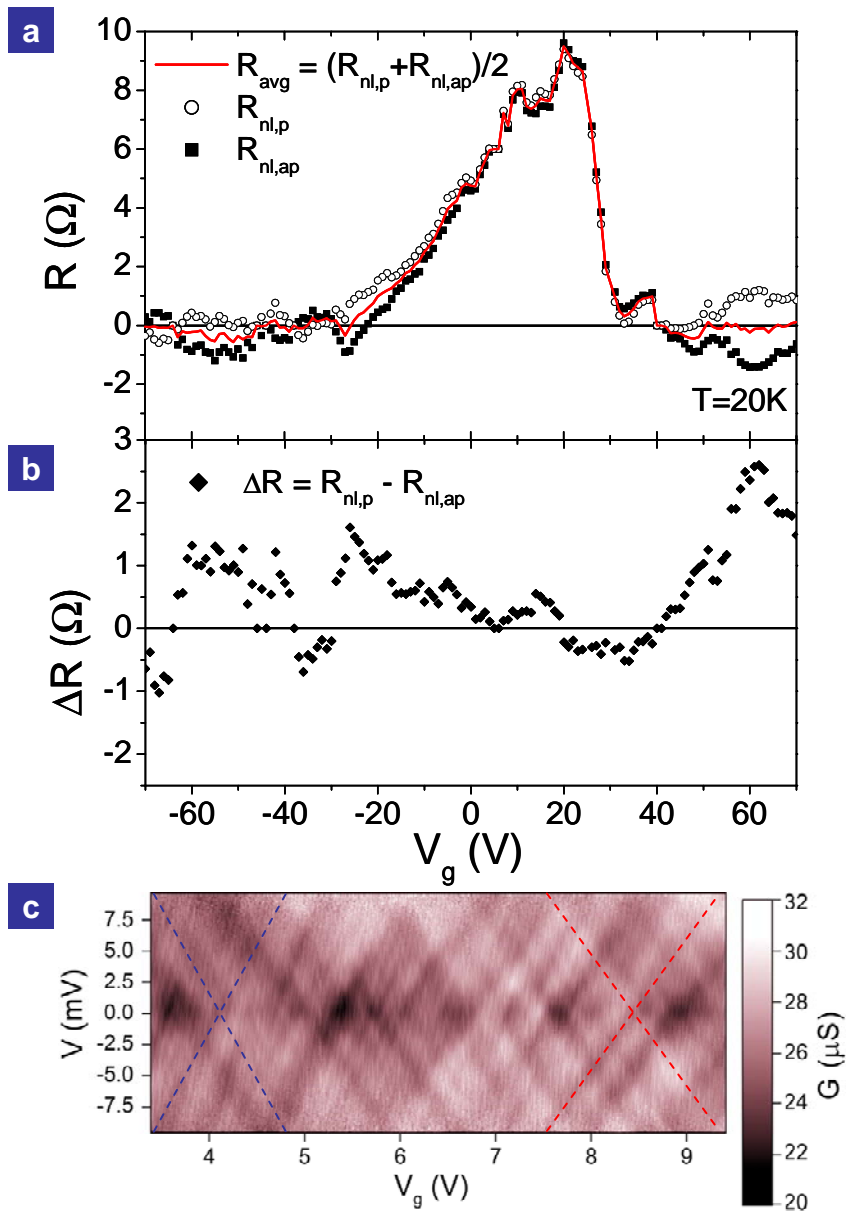


Figure 4

